26. MegAlign program, DNASTAR, Madison, WI.
27. L. Redmond, S.-R. Oh, C. Hicks, G. Weinmaster, A. Ghosh, *Nature Neurosci.* **3**, 30 (2000).
28. To create the CREST antibody, We used PCR to amplify full-length *crest* cDNA from P0 mouse brain total RNA and cloned it into pET21 vector for expression of His-tagged CREST protein in bacteria. After isopropyl-β-D-thiogalactopyranoside induction, CREST protein was mainly collected in the inclusion body of the bacteria and extracted with 6 M urea. We further purified the protein with Ni-NTA agarose fractionation. After SDS–polyacrylamide gel electrophoresis (PAGE), the Coomassie brilliant blue–stained CREST band was excised and injected into rabbits to produce anti-CREST antiserum.
29. To generate the *crest* knockout mice, *crest* genomic DNA was cloned by screening a 129SVJ mouse genomic phage library (gift of A. Kolodkin) with full-length mouse *crest* cDNA as a probe. After mapping the restriction enzyme sites, we generated a knockout vector with a Neo gene cassette (Fig. 4). We deleted the poly(A) addition signal from the Neo gene cassette for poly(A) trapping method of gene targeting. The cassette replaced all of exon 4 and a 5′ portion of exon 5. ES cells transfected with the targeting vector and resistant to G418 and gancyclovir were expanded and screened by genomic Southern blotting. Correctly targeted ES cells were injected into C57B6J-derived blastocysts and resulted in the generation of several high-percentage chimeras, which produced germline targeted offspring. Genotyping of mice was performed on tail clip DNA by PCR.
30. We thank D. Livingston for the UAS-CAT construct; A. Lanahan for advice on library construction; A. Kolodkin for rat phage libraries; L. Redmond, A. Datwani, K. Whitford, M.-R. Song, and G. Ince for various procedures; J. Nathans, C. Montell, D. Ginty, P. Worley, S. Snyder, D. Linden, D. Murphy, P. Kim, M. Molliver for discussions; and M. Greenberg, D. Ginty, A. Kolodkin, and S. Snyder for comments on the manuscript. Supported by grants from NIH (MH60598 and NS39993), the March of Dimes Birth Defects Foundation (A.G.), the Klingenstein Foundation (A.G.), and a Merck Scholar Award (A.G.). H.A. was supported by a Uehara Memorial Foundation Research Fellowship.

Supporting Online Material
www.sciencemag.org/cgi/content/full/303/5655/197/DC1
Materials and Methods
Figs. S1 to S3

30 July 2003; accepted 28 October 2003

^{14}C Activity and Global Carbon Cycle Changes over the Past 50,000 Years

K. Hughen,[1]* S. Lehman,[3] J. Southon,[4] J. Overpeck,[5,6] O. Marchal,[2] C. Herring,[1] J. Turnbull[3]

A series of ^{14}C measurements in Ocean Drilling Program cores from the tropical Cariaco Basin, which have been correlated to the annual-layer counted chronology for the Greenland Ice Sheet Project 2 (GISP2) ice core, provides a high-resolution calibration of the radiocarbon time scale back to 50,000 years before the present. Independent radiometric dating of events correlated to GISP2 suggests that the calibration is accurate. Reconstructed ^{14}C activities varied substantially during the last glacial period, including sharp peaks synchronous with the Laschamp and Mono Lake geomagnetic field intensity minimal and cosmogenic nuclide peaks in ice cores and marine sediments. Simulations with a geochemical box model suggest that much of the variability can be explained by geomagnetically modulated changes in ^{14}C production rate together with plausible changes in deep-ocean ventilation and the global carbon cycle during glaciation.

Radiocarbon age may deviate significantly from calendar age as a result of time-varying processes affecting ^{14}C production in the atmosphere, as well as the distribution of ^{14}C among the active global carbon reservoirs (*1*). To account for such changes, radiocarbon age determinations must be calibrated against independent estimates of calendar age, but existing calibration data sets often lack temporal range and/or resolution. The current standard calibration, Intcal98 (*2*), extends at high resolution back to just ~14,600 calendar years before the present (14.6 cal. ka B.P.) on the basis of annual tree rings (*3*) and varved (annually layered) marine sediments (*4*). Paired ^{14}C and U/Th ages on corals (*5*) provide additional calibration points back to ~40 cal. ka B.P., but at much lower resolution. Varved lake sediments (*6*), U/Th ages on speleothems (*7*) and lake sediments (*8*), and marine sediments correlated to Greenland ice core chronologies (*9*, *10*) have also been used to constrain calibration and initial ^{14}C activity [expressed as Δ^{14}C (*11*)] beyond the range of Intcal98. In many cases, these records suggest that extremely large and rapid shifts in Δ^{14}C have occurred; however, these records also show disagreements before ~25 cal. ka B.P. that are as large as the reconstructed anomalies. Thus, considerable uncertainty remains in calibrating the older half of the ^{14}C time scale. Here, we present a calibration and reconstruction of Δ^{14}C back to 50 cal. ka B.P. on the basis of the correlation of ^{14}C data from Cariaco Basin sediments with the annual-layer time scale of the GISP2 Greenland ice core (*12*). Similarity between reconstructed Δ^{14}C and variations in ^{14}C production rate estimated from independent paleomagnetic and geochronologic data suggests that the calibration and Δ^{14}C reconstruction are accurate despite the lack of in situ calendric age control.

[1]Department of Marine Chemistry and Geochemistry, [2]Department of Geology and Geophysics, Woods Hole Oceanographic Institution (WHOI), Woods Hole, MA 02543, USA. [3]Institute of Arctic and Alpine Research, University of Colorado, Boulder, CO 80309, USA. [4]Department of Earth System Science, University of California, Irvine, CA 92697, USA. [5]Department of Geosciences, [6]Institute for the Study of Planet Earth, University of Arizona, Tucson, AZ 85721, USA.

*To whom correspondence should be addressed. E-mail: khughen@whoi.edu

Our ^{14}C series (Fig. 1) is constructed from 280 accelerator mass spectrometry (AMS) ^{14}C measurements on planktonic foraminifera extracted from discrete sediment samples in holes 1002D and 1002E from Ocean Drilling Program (ODP) leg 165, site 1002, in the Cariaco Basin (10°42.73′N, 65°10.18′W, 893-m water depth). The results span a ^{14}C age range of 55 to 12 ka B.P. and complement 355 varve-age calibrated ^{14}C measurements for the interval from ~15 to 10 cal. ka B.P. based on our prior studies of nearby Cariaco Basin sediment piston cores (*4*, *13*). AMS ^{14}C target preparation and measurement was conducted at three different institutions: Center for Accelerator Mass Spectrometry at Lawrence Livermore National Laboratory (CAMS-LLNL) (n = 127), Laboratory for AMS Radiocarbon Preparation and Research at University of Colorado, Boulder, and National Ocean Sciences AMS at WHOI (NSRL-NOSAMS) (n = 118), and the Keck CCAMS Facility at University of California, Irvine (n = 35) (Fig. 1 and table S1) (*14*). A constant 420-year marine reservoir age correction (difference between ^{14}C ages of surface water and atmosphere) was applied to all ^{14}C ages, in accordance with prior studies demonstrating that the local Cariaco Basin reservoir age has varied little, even when climate conditions and forcings have changed dramatically (*14*).

The initial ^{14}C chronology for hole 1002D showed a large age reversal from 14 to 14.5 meters below the sea floor (mbsf) (Fig. 1), in association with the boundary between successive 10-m core sections. We therefore performed additional measurements across the equivalent interval in adjacent hole 1002E, which was drilled in offsetting fashion. Magnetic susceptibility records were used to identify the disturbed section in 1002D and to align the two holes (fig. S1). The ^{14}C dates for undisturbed sections in both holes agree closely, but results from hole 1002E do not display a large age reversal (Fig. 1, inset) and were thus used to bridge the disturbed section.

Calendar age chronology. Our prior studies of Cariaco Basin sediments made use of annual varve counts to compare timing of abrupt changes in upwelling proxies to calendrically

dated instrumental and proxy temperature records in the high-latitude North Atlantic region and indicated that correlative climate changes occurred within 1 year during the past 110 years (*15*) and within 1 decade during the last deglaciation (*13*, *16*). Laminations are not present continuously, however, across the longer interval of the current study (*17*). Therefore, calendar age estimates for the new composite ^{14}C record were derived by transferring ages from the GISP2 ice core to Cariaco Basin site 1002 sediments with the use of the correlation of climate proxies from the two sites (fig. S2). Implicit to this approach is the assumption that the near-synchronous coupling between climate changes at Cariaco Basin and Greenland observed during the last deglaciation (*13*, *16*) and seen in general circulation model simulations (*18*) also existed during earlier millennial-scale events.

Precision of the calendar time scale derived in this way has two sources of uncertainty, one pertaining to derivation of the GISP2 time scale itself and another related to correlation between records. Annual layer counts in the GISP2 ice core were used back to about 40 cal. ka B.P. (*12*), but a less precise correlation to the orbitally tuned SPECMAP marine $\delta^{18}O$ record was used beyond that point. Estimated error in the GISP2 chronology is ±2% back to ~39.9 cal. ka B.P. but increases to ±5% by 44.6 cal. ka B.P. and ±10% by 56.9 cal. ka B.P. (*12*). Uncertainties in the correlation procedure between GISP2 and Cariaco records result in an additional calendar-age error that is estimated to be ±180 years (*14*). Possible errors in the GISP2 chronology itself are not independent from point to point but would affect the sequence as a whole. Offsets between different Greenland ice-core age models do not accumulate uniformly in the glacial, but appear over relatively short sections of core at maximum rates of about ±200 years per 1000 years (*19*). We take this as an upper bound for possible ice core errors and an indication that sections of the Cariaco calibration data set may need to be stretched or compressed within these limits if parts of the GISP2 chronology are incorrect. As discussed later, these changes are insufficient to alter the millennial-scale features of the calibration and implied $\Delta^{14}C$.

Accuracy of the GISP2 layer-counting chronology is supported by radiometric dating of correlative records. Calcite $\delta^{18}O$ from Hulu Cave in eastern China (*20*) and $\delta^{13}C$ from Villars Cave in southwest France (*21*) show distinct millennial-scale events during the last glacial period that can be reliably correlated with the GISP2 record. U/Th dates for both caves agree within errors with GISP2 layer counts for the interval from 10 to 40 cal. ka B.P. (*20*, *21*). In addition, records of cosmogenic nuclide flux in GISP2 and Greenland Ice Core Project (GRIP) ice cores show large peaks in ^{10}Be and ^{36}Cl (*22*) that occurred at ~41 cal. ka B.P. and ~34 cal. ka B.P., according to the GISP2 age model. These have been correlated with marine sedimentary evidence of geomagnetic field intensity minima identified as the Laschamp and Mono Lake excursions, respectively (*23*). Published K-Ar and Ar-Ar dates for the Laschamp excursion [(*24*) and references therein] vary widely about a mean of ~45 cal. ka B.P. However, recent Ar-Ar dates on Laschamp-correlative tephras yielded ages of 39.4 ± 0.1 (*25*) and 41.1 ± 2.1 cal. ka B.P. (*24*), in closer agreement with the GISP2 age.

^{14}C calibration. A plot of ^{14}C versus GISP2 calendar age for Cariaco sediments provides a ^{14}C calibration from 50 to 15 cal. ka B.P. (Fig. 2). The record shows prominent ^{14}C age plateaus at ~33, ~28, ~24, and ~13.3 ^{14}C ka B.P. There is an abrupt shift at 42 to 40 cal. ka B.P. away from the 1:1 line, followed by a general trend of decreasing calendar-^{14}C age offset from ~40 to 15 cal. ka B.P. The abrupt shift at ~42 to 40 cal. ka B.P. represents the largest structural feature in the curve, with nearly 7000 ^{14}C years elapsing in only 2000 calendar years. The Cariaco record agrees well with numerous coral U/Th-^{14}C age pairs back to 24 cal. ka B.P. and single points at ~30 and ~41 cal. ka B.P. (*5*) (Fig. 2A), providing support for the accuracy of the calibration, at least back to ~41 cal. ka B.P. Comparison of Cariaco data to other published ^{14}C–calendar age data sets places the Cariaco record near the center of the distribution (Fig. 2B) and in general agreement with previous records based on marine sediments (*9*, *10*). The Lake Suigetsu record (*6*) shows younger calendar and/or older ^{14}C ages, whereas the Bahama speleothem record (*7*) shows older calendar and/or younger ^{14}C ages. The cause of the offsets between these records remains uncertain, but general similarity of ^{14}C structure, such as the rapid change from 41 to 34 ^{14}C ka B.P. and the large plateau at 28 ^{14}C ka B.P., suggests that the discrepancies are because of differences in the calendar chronologies and not the ^{14}C ages.

Reconstructed $\Delta^{14}C$, geomagnetism, and carbon cycle dynamics. The $\Delta^{14}C$ values calculated from the Cariaco calibration data (Fig. 3) show a rapid shift from the lowest values of the record, centered at ~46 cal. ka B.P., to the highest values, at ~40 cal. ka B.P. In addition to the peak at ~40 cal. ka B.P., there are prominent peaks at ~34, ~29, and ~17 cal. ka B.P. and minima centered at ~36 and ~31 cal. ka B.P., superimposed on generally elevated values during the glacial period from 40 to 16 cal. ka B.P. Changes in $\Delta^{14}C$ arise from varia-

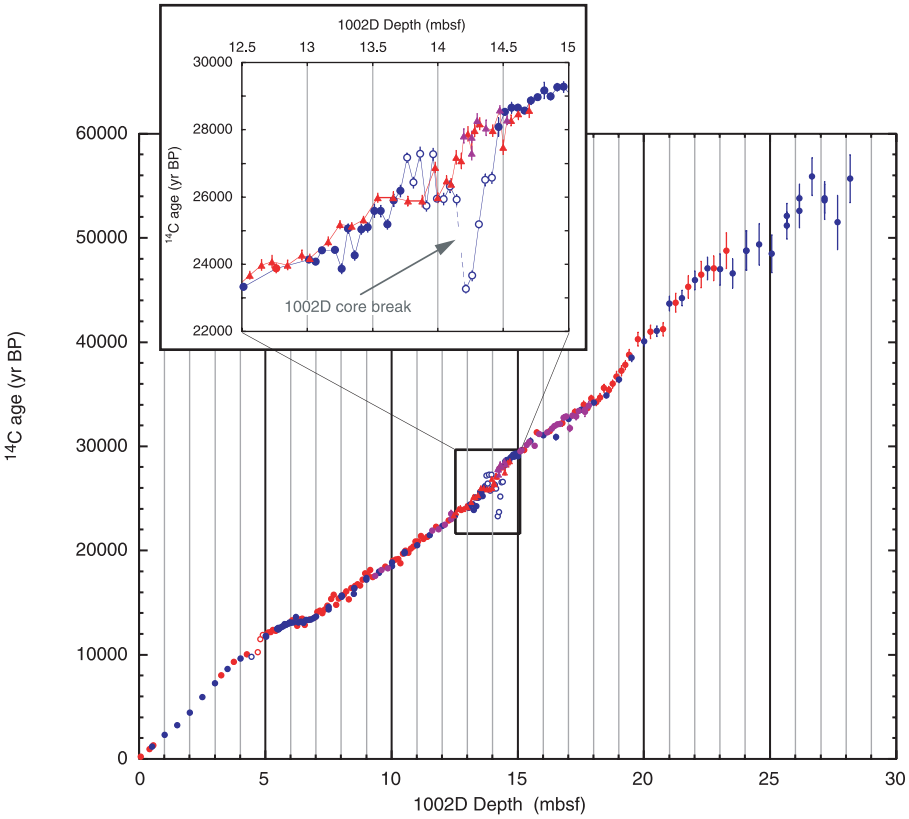

Fig. 1. AMS ^{14}C dates for Cariaco ODP leg 165, holes 1002D and 1002E, plotted versus depth in mbsf. Circles indicate samples from hole 1002D; triangles are from hole 1002E. Blue data points were generated at CAMS-LLNL, red points are from NSRL-NOSAMS, and purple points are from University of California, Irvine. Open symbols show dates taken from sediments at core breaks that were likely disturbed during extraction of successive 10-m core sections. Error bars are 1 σ (*14*). (**Inset**) Detail of ^{14}C results from 12.5 to 15 mbsf showing disturbed section of hole 1002D that was bridged by correlating magnetic susceptibility records with undisturbed hole 1002E (fig. S1).

tions in the rate of ^{14}C production as well as altered size of and/or exchange between active carbon reservoirs. The "solar wind" stream of charged particles from the sun modulates the production of ^{14}C in the atmosphere on brief time scales. At the scale of $\geq 10^2$ years, changes in intensity of Earth's dipole field may modulate ^{14}C production by a factor of two to three (*26*, *27*), and recent evidence from marine sediments reveals greatly varying geomagnetic intensity in the past that is thought to represent widespread changes in field strength (*23*). Figure 4A shows an estimate of ^{14}C production for the past 50 ka B.P. based on a revised high-resolution paleointensity compilation for the North Atlantic, NAPIS-75 (*23*), and the relation of ^{14}C production and geomagnetic intensity (I/I_0) modeled by Masarik and Beer (*27*). The NAPIS-75 calendar-age model has its basis in correlation of associated climate proxy data with the GISP2 climate record and is thus directly comparable to that for the Cariaco Basin. The estimated ^{14}C production and Cariaco Basin $\Delta^{14}C$ series are strikingly similar (Fig. 4), both showing a dramatic increase from 44 to 40 cal. ka B.P.; discrete peaks during the Laschamp, Mono Lake, and an unnamed geomagnetic event at ~40, ~34, and ~29 cal. ka B.P., respectively; and deep minima at ~48 to 44, ~36, and ~33 to 31 cal. ka B.P. These similarities cannot be attributed to common derivation of the calendar age models alone but must also reflect the modulation of both $\Delta^{14}C$ and regional geomagnetic intensity by changes in strength of Earth's dipole field. Possible errors in the GISP2 calendar age model, even if concentrated over brief intervals (e.g., *19*), would result in estimated $\Delta^{14}C$ shifts of only ~40 per mil (‰) over 1000 years (i.e., an order of magnitude smaller than the main features of the Cariaco record).

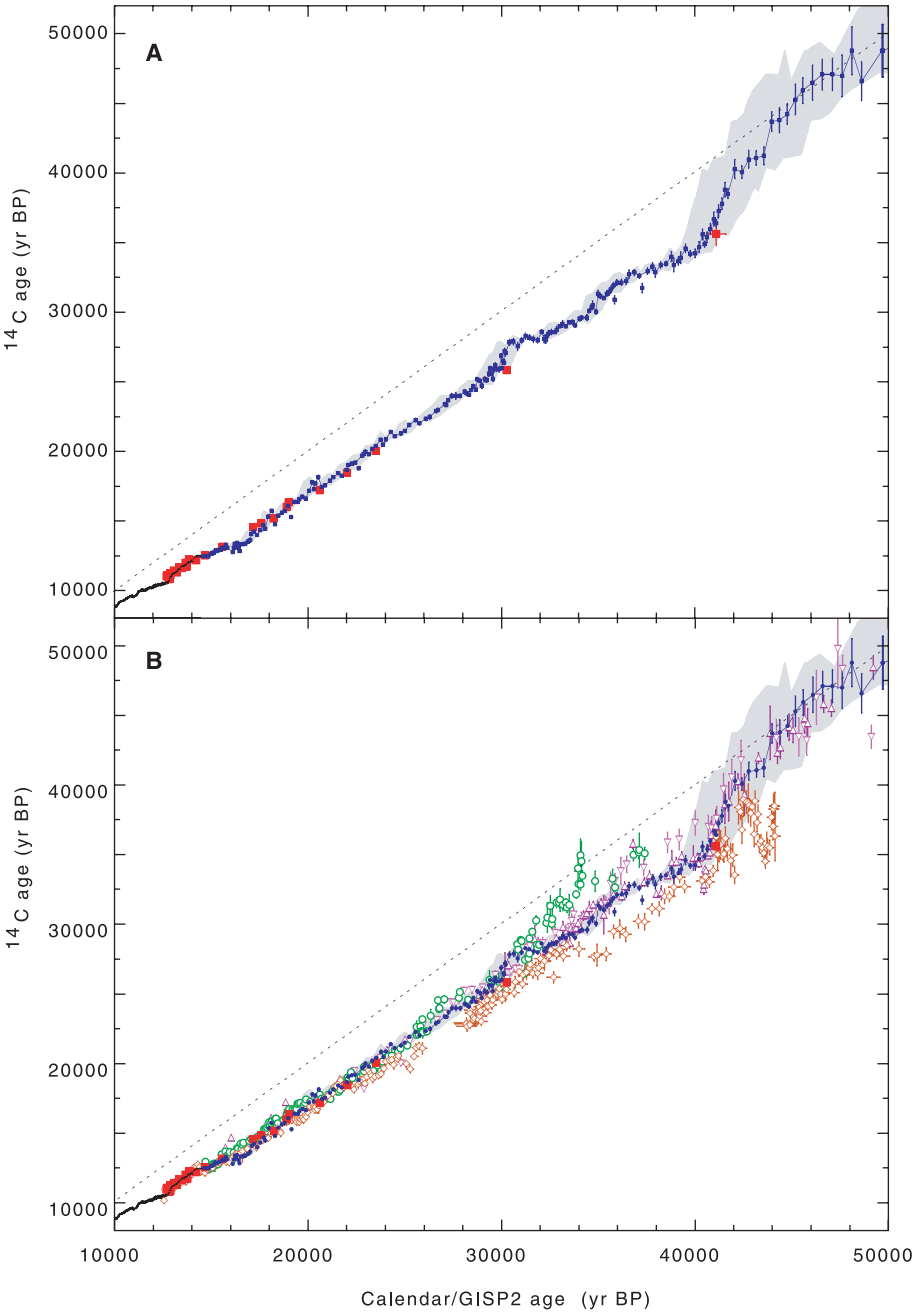

Fig. 2. Radiocarbon calibration data from various sources. (**A**) Calibration data from Cariaco leg 165, holes 1002D and 1002E (blue circles), plotted versus GISP2 calendar age (*12*) assigned by correlation of detailed paleoclimate records (*17*) (SOM Text and fig. S2). The thin black line is high-resolution calibration data from Intcal98 tree rings (*2*, *3*) joined at ~12 cal. ka B.P. to the Cariaco PL07-58PC varve chronology (*13*). Red squares are paired ^{14}C-U/Th dates from corals (*5*). Replicate measurements, including overlap between 1002D and 1002E, have been averaged. Light gray shading represents the Cariaco calibration curve shifted within limits of calendar age uncertainty. Dashed line shows equal ^{14}C-calendar ages. Error bars are 1 σ. (**B**) Cariaco site 1002 data set plotted versus other published ^{14}C calibration data. Symbols are the same as above, with additional data from Lake Suigetsu varves (*6*) (open circles), Bahama speleothem U/Th (*7*) (open diamonds), and North Atlantic cores PS2644 (*9*) (upside-down triangles) and SO82-5 (*10*) (triangles) correlated to GISP2. Error bars for all records are 1 σ.

In order to evaluate the contribution of geomagnetically modulated changes in production rate to variations in reconstructed $\Delta^{14}C$, we carried out sensitivity tests with the use of a geochemical box model of the global carbon cycle. The model consists of seven reservoirs: the atmosphere, terrestrial biota plus soils/detritus, surface and deep oceans, and shallow and deep marine sediments containing organic and inorganic carbon (fig. S3). Reservoir inventories and exchange fluxes were specified from consensus estimates for the preindustrial carbon cycle (*14*).

We adopt the contemporary ^{14}C production rate of 2.02 atom cm^{-2} s^{-1} of Masarik and Beer (*27*), which is in the middle of the range of previous estimates [Supporting Online Material (SOM) Text]. As noted by others (*7*, *28*), however, the global integral of all but the lowest production rate estimates exceeds the observed sum of ^{14}C decays in active reservoirs. We therefore follow Damon and Sternberg (*28*) in specifying additional sedimentation of carbon into long-lived reservoirs as needed to balance ^{14}C production. For simplicity, the additional sedimentation is assumed to be entirely marine, with an inorganic- to organic-carbon burial ratio of 4:1 as needed to satisfy a steady-state ocean $\delta^{13}C$ constraint (SOM Text). With this adjustment, the box model produced ocean, atmosphere, and terrestrial biosphere ^{14}C activities in agreement with the a priori consensus estimates. The model was then used to simulate atmospheric $\Delta^{14}C$ changes in response to 50 ka B.P. of changing ^{14}C production as determined from the revised NAPIS-75 paleointensity stack (Fig. 4A) (*29*). We confirm previous findings of overall agreement between simulated and observed atmospheric $\Delta^{14}C$ for the Holocene period but

observed values that are significantly higher than simulated values for the remainder of the record (Fig. 4B, curve a) (*23*). This offset is most likely attributable to altered carbon cycle dynamics during the glacial period [e.g., (*23*)].

To represent such changes, we performed a second simulation with the atmosphere and terrestrial biosphere reduced to 75% and 65% of their preindustrial carbon inventories, respectively (*30*). Atmospheric $\Delta^{14}C$ in this simulation increases only slightly (+10 to 30‰) (Fig. 4B, curve b) because of diminished dilution of ^{14}C by stable carbon. In a third simulation, the reduced atmosphere and biosphere inventories were maintained, and we included a 50% reduction of surface–deep ocean exchange in order to represent the possible reduction of North Atlantic Deep Water (NADW) formation during the glacial period (*31*). This "reduced carbon cycle" simulation produces substantially higher atmospheric activity than the full carbon cycle (+100 to 200‰) for the same ^{14}C production rate history (Fig. 4B, curve c), primarily because of reduced transfer of ^{14}C into the ocean interior, where most global ^{14}C decay occurs. Simulated atmospheric $\Delta^{14}C$ arising from these combined changes is nevertheless below observed values for parts of the glacial period. We therefore performed a final simulation with the same reductions as above but also including a decrease in the surface marine $CaCO_3$ sediment flux to 10% of its preindustrial value to represent the abandonment of coral reefs during periods of low glacial sea level (*32*). In the model, this has the effect of shifting ^{14}C out of the surface sediment sink and into ocean reservoirs exchanging with the atmosphere. Under these "minimum carbon cycle" boundary conditions, which probably represent an upper limit of reasonable perturbations to the global carbon cycle, simulated $\Delta^{14}C$ is generally ~150‰ higher than that for the "reduced carbon cycle" with decreased ocean ventilation and brackets all but the highest glacial-age observations (Fig. 4B, curve d) (SOM Text). We note that reducing vertical mixing in the ocean by 50% and reducing shallow carbonate sedimentation by 90% have comparable effects on atmospheric $\Delta^{14}C$ in our simple model. However, the imbalance between carbonate ion input and deposition arising from reduced carbonate sedimentation can only be maintained for several thousand years before carbonate compensation restores the system to equilibrium. On the other hand, reduced vertical exchange in the ocean can be maintained for much or all the glacial period and must have contributed importantly to long-term amplification of the atmospheric $\Delta^{14}C$ signal.

Discussion. The large variability in Cariaco $\Delta^{14}C$ from ~50 to 15 cal. ka B.P. appears to reflect geomagnetically modulated changes in production rate that are amplified by diminished ^{14}C sinks during glacial times, as suggested by others (*7*, *23*). The Laschamp and Mono Lake geomagnetic excursions are well represented in the Cariaco $\Delta^{14}C$ record, in agreement with other cosmogenic nuclide records from sediments and ice cores. In addition, distinct $\Delta^{14}C$ minima around ~36 and ~32 cal. ka B.P., and a subsequent peak at ~29 cal. ka B.P., are also present in geomagnetic data, providing a possible explanation for much of the observed $\Delta^{14}C$ variability. An exception is seen in the negative $\Delta^{14}C$ values observed from ~48 to 44 cal. ka B.P., which are not consistent with modeled $\Delta^{14}C$ in the range of +100‰ (Fig. 4). Error bars for $\Delta^{14}C$ may mitigate the discrepancy somewhat (Fig. 3), but systematic ^{14}C measurement errors in one direction are unlikely. A more probable explanation is that the GISP2 age model underestimates calendar ages older than about 40 cal. ka B.P., where the layer-counting part of the chronology ends (*12*). A revised time scale for the nearby GRIP ice core (*19*) is consistent with the GISP2 chronology over the period 40 to 10 cal. ka B.P., but increases in age more rapidly beyond ~40 cal. ka B.P. and is more than 2000 years older than GISP2 at ~50 cal. ka B.P. (*19*). Adoption of this revised GRIP chronology beyond the range of GISP2 layer counting would increase $\Delta^{14}C$ over the period from 43 to 50 cal. ka B.P. by more than +200‰, greatly improving the match with modeled $\Delta^{14}C$.

Reconstructed $\Delta^{14}C$ values exceed those for the "reduced carbon cycle" simulation (Fig. 4, curve c) during several intervals. For example, high values from 18 to 16 cal. ka B.P. in Cariaco $\Delta^{14}C$ are not predicted from the geomagnetic estimates of ^{14}C production. The timing of this $\Delta^{14}C$ maximum coincides with Heinrich event 1 (H1), which involved a major influx of glacial meltwater to the North Atlantic Ocean that may have reduced ocean ventilation to levels below the glacial mean state (*33*, *34*). Peaks in $\Delta^{14}C$ are also reconstructed at ~40 and ~29 cal. ka B.P. and previously reported at ~12 cal. ka B.P. (*13*), coincident with Heinrich events H4, H3, and H0 (Younger Dryas), respectively (*35*). These events may also have been associated with unusually large perturbations in ocean ventilation and sea-ice cover explaining "anomalously" elevated $\Delta^{14}C$ at those times (*23*, *36*). We note that observed $\Delta^{14}C$ increases at ~40 and ~29 cal. ka B.P. appear out of proportion to their respective modeled, geomagnetically modulated $\Delta^{14}C$ increases (relative, for example, to ~34 cal. ka B.P.) (Fig. 4). It is possible that coincident timing of reduced deep-ocean ventilation during Heinrich events and peaks in geomagnetic ^{14}C production (*23*) may have contributed to producing exceptionally large increases in $\Delta^{14}C$ during both of those intervals.

Large variations in $\Delta^{14}C$, similar to the Cariaco record, are observed from ~43 to 33 cal. ka B.P. in a Bahama speleothem record (*7*), but

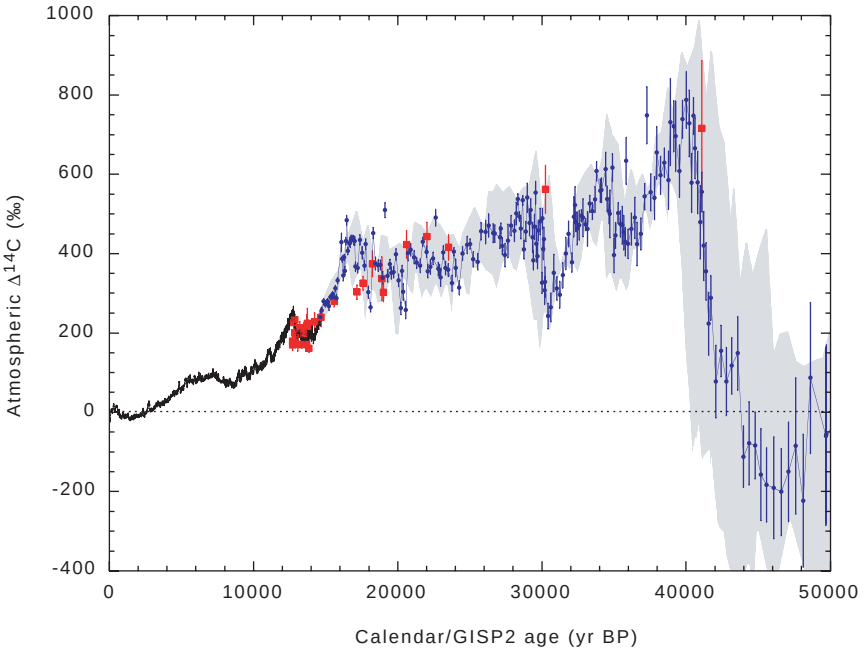

Fig. 3. Atmospheric $\Delta^{14}C$ for the past 50 cal. ka B.P. Symbols are the same as those in Fig. 2A. Cariaco error bars represent independent uncertainty in $\Delta^{14}C$ due to 1-σ ^{14}C age error. Light gray shading shows additional uncertainty in Cariaco $\Delta^{14}C$ due to calendar-age error that is not independent from sample to sample, but rather would shift sections of the curve together within the limits of the shading. Dotted line is modern preindustrial atmospheric $\Delta^{14}C$, defined as 0‰. Upper and lower limits were determined by adding and subtracting 1–σ errors to the calendar age and recalculating $\Delta^{14}C$ with the use of the new calendar ages.

reconstructed $\Delta^{14}C$ for that record reaches ~1000 to 1300‰. The magnitude and duration of such implied $\Delta^{14}C$ values are difficult to explain with available geomagnetic records and plausible carbon cycle changes. For example, to achieve sustained atmospheric $\Delta^{14}C$ of 1000 to 1200‰ in our model, the "minimum carbon cycle" parameters must be maintained (despite the temporal "carbonate compensation" constraint) and global deep ocean ventilation must be reduced by 85%. Simulating an implied ~1300‰ peak in the speleothem record at ~44 cal. ka B.P. required Beck *et al*. (*7*) to arbitrarily set the geomagnetic and solar magnetic fields to zero field strength, in addition to specifying large reductions in the carbon cycle. Many of the features of the Cariaco record, on the other hand, can be reproduced with the use of plausible changes to the global carbon cycle and published estimates of geomagnetic field strength. Although the individual simulations do not match all of the details of the Cariaco reconstruction, the fact that time-invariant "full," "reduced," and "minimum" carbon cycle parameters yield results that bracket the observed values implies that changing the carbon cycle within these established limits [i.e., similar to the time-variant approach used by Laj *et al.* (*23*)] would allow us to explain much of the record.

Finally, the striking similarity of the geomagnetically derived record of ^{14}C production and the Cariaco $\Delta^{14}C$ reconstruction suggests that unexplained differences between simulated $\Delta^{14}C$ and the observations may be attributable to remaining weaknesses in our understanding and modeling of the carbon cycle (i.e., dampening the production signal excessively). Alternatively, the relationship of production rate as a function of geomagnetic intensity may be steeper at low intensities than that indicated by Masarik and Beer (*27*) (SOM Text).

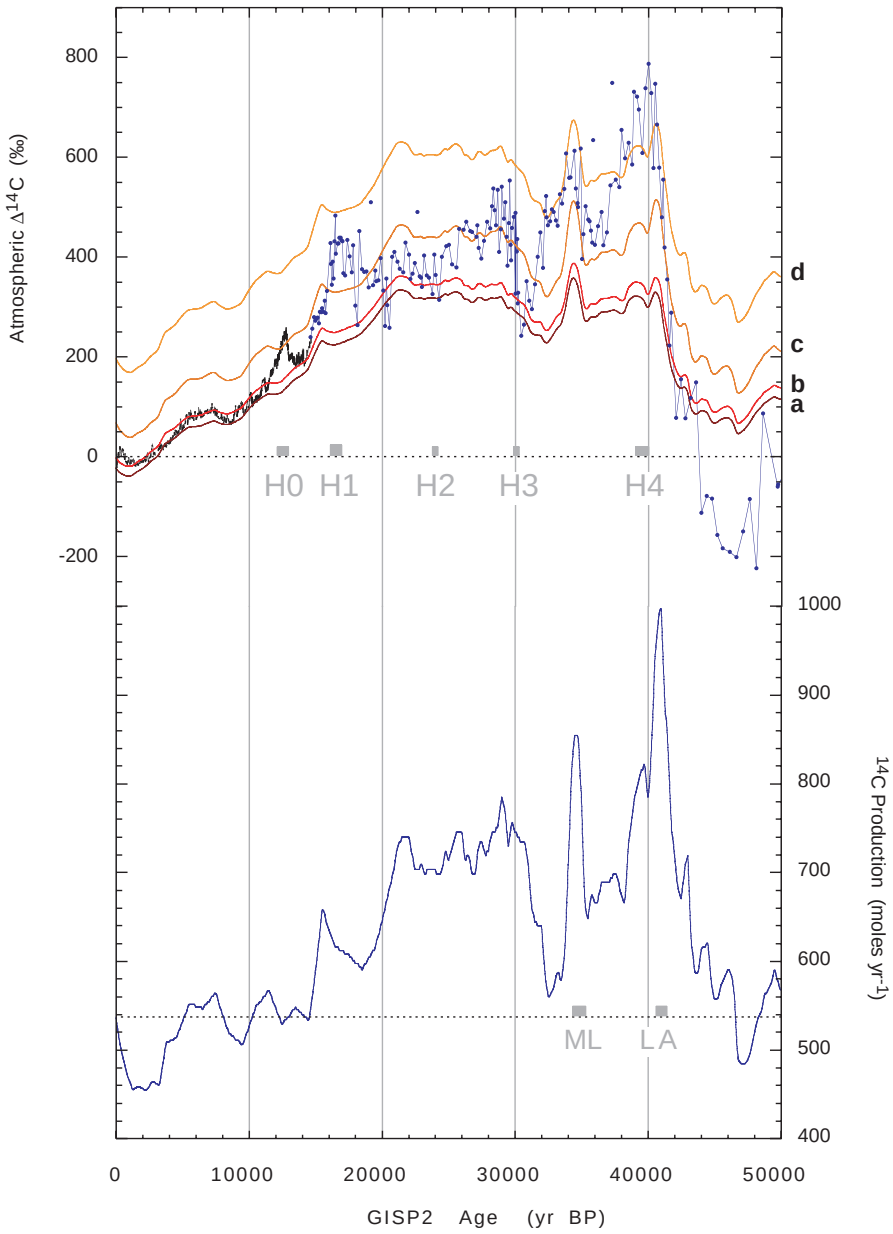

Fig. 4. (Lower Curve) Global ^{14}C production, calculated as a function of the earth's geomagnetic field intensity (*23*) with the use of the equation of Masarik and Beer (*27*) and plotted versus GISP2 calendar age. The Laschamp (LA) and Mono Lake (ML) geomagnetic field minima (production maxima) are indicated at ~35 and ~41 cal. ka B.P. Dotted line indicates modern preindustrial ^{14}C production (537 moles year^{-1}) (*27*). (Upper Curves) Comparison of observed Cariaco site 1002 atmospheric $\Delta^{14}C$ record to atmospheric $\Delta^{14}C$ calculated by a seven-box model of the active global carbon cycle. Cariaco 1002D-E (solid circles) and Intcal98/Cariaco58PC (thin line) data are plotted without error bars for clarity. Curves a to d show box model simulations of different carbon cycle boundary conditions (see SOM Text, fig. S3, and table S2 for details). The model simulations are all forced with the same annual ^{14}C production shown in the lower curve. Curve a shows atmospheric $\Delta^{14}C$ simulated for the past 50 cal. ka B.P. with the use of modern preindustrial "full carbon cycle" boundary conditions; curve b, glacial boundary conditions with diminished carbon reservoirs in the atmosphere and biosphere ("reduced Atm/Bio carbon cycle"). Curve c is the same as b, but including a 50% reduction in surface–deep ocean exchange flux ("reduced Atm/Bio/THC carbon cycle"); curve d, same as for c, but also including reduced flux into shallow marine carbonate sediments by 90% ("minimum carbon cycle"). Approximate timing (*35*) of Heinrich events H4 through H0 shown by gray bars.

References and Notes

1. "Active" refers here to those reservoirs that exchange carbon on time scales of 10^1 to 10^4 years.
2. M. Stuiver *et al*., *Radiocarbon* **40**, 1041 (1998).
3. B. Kromer, M. Spurk, *Radiocarbon* **40**, 1117 (1998).
4. K. A. Hughen *et al*., *Nature* **391**, 65 (1998).
5. E. Bard *et al*., *Radiocarbon* **40**, 1085 (1998).
6. H. Kitigawa, J. Van der Plicht, *Science* **279**, 1187 (1998).
7. J. W. Beck *et al*., *Science* **292**, 2453 (2001).
8. A. Schramm, M. Stein, S. L. Goldstein, *Earth Planet. Sci. Lett.* **175**, 27 (2000).
9. A. H. L. Voelker, P. M. Grootes, M.-J. Nadeau, M. Sarnthein, *Radiocarbon* **42**, 437 (2000).
10. S. van Kreveld *et al*., *Paleoceanography* **15**, 425 (2000).
11. The $\Delta^{14}C$, expressed in ‰, is calculated as $(Fm \times e^{\lambda t} - 1) \times 1000$, where Fm is the fraction of modern ^{14}C after marine reservoir correction, λ is the true ^{14}C decay constant, and t is the calendar age (*37*).
12. D. A. Meese *et al*., *J. Geophys. Res.* **102**, 26411 (1997).
13. K. A. Hughen, J. R. Southon, S. J. Lehman, J. T. Overpeck, *Science* **290**, 1951 (2000).
14. Materials and methods are available as supporting material on *Science* Online.
15. D. E. Black *et al*., *Science* **286**, 1709 (1999).
16. K. A. Hughen, J. T. Overpeck, L. C. Peterson, S. Trumbore, *Nature* **380**, 51 (1996).
17. L. C. Peterson, G. H. Haug, K. A. Hughen, U. Rohl, *Science* **290**, 1947 (2000).
18. D. Rind, D. Peteet, W. S. Broecker, A. McIntyre, W. Ruddiman, *Clim. Dyn.* **1**, 3 (1986).
19. S. Johnsen *et al*., *J. Quat. Sci.* **16**, 299 (2001).
20. Y. J. Wang *et al*., *Science* **294**, 2345 (2001).
21. D. Genty *et al*., *Nature* **421**, 833 (2003).
22. J. Beer *et al*., *Quat. Sci. Rev.* **21**, 1129 (2002).
23. C. Laj *et al*., *Earth Planet. Sci. Lett.* **200**, 177 (2002).
24. T. Ton-That, B. Singer, M. Paterne, *Earth Planet. Sci. Lett.* **184**, 645 (2001).
25. P. B. Gans *et al*., *Geol. Soc. Am. Abstr. Programs* **31**, 56 (1999).
26. D. Lal, in *Solar-Terrestrial Relationships and the Earth Environment in the Last Millenia*, vol. 95 of *Proceedings of the International School of Physics, Enrico Fermi* (North Holland, Bologna, Italy, 1988), p. 216.
27. J. Masarik, J. Beer, *J. Geophys. Res.* **104**, 12,099 (1999).

28. P. E. Damon, R. E. Sternberg, *Radiocarbon* **31**, 697 (1989).
29. The same experiment was performed with the use of a zonally averaged global ocean circulation model with atmospheric and biospheric carbon exchange as described in (*38*). The more detailed model produced atmospheric $\Delta^{14}C$ for the past 50 ka B.P. within ±10‰ of the simple box model. Subsequent glacial perturbation experiments were carried out in the box model as a computational expedient.
30. Measurements of air bubbles in ice cores show that glacial atmospheric CO_2 concentration averaged ~200 parts per million by volume (ppmv) compared to a preindustrial value of ~280 ppmv (*39*). A reduction of terrestrial biomass to 65% of its preindustrial size is within the bounds of previous estimates (*40*) and is necessary to balance a lowering of glacial $\delta^{13}C$ of oceanic ΣCO_2 by an average of −0.3‰ (*41*).
31. Reduced deep-ocean ventilation is consistent with potentially restricted NADW formation and penetration in the glacial ocean. Global transects of radiocarbon distribution in the oceans suggest that NADW formation is responsible for sequestering up to 75% of the radiocarbon in the deep ocean (*42*).
32. This change represents a 120-m lowering of sea level and the resultant shift of carbonate sedimentation off the continental shelves into deep water, where dissolution is much more extensive. Discussion and details of the glacial carbon cycle boundary conditions are summarized in SOM Text, fig. S3, and table S2.
33. L. D. Keigwin, S. J. Lehman, *Paleoceanography* **9**, 185 (1994).
34. J. F. McManus, R. Francois, J.-M. Gherardi, L. D. Keigwin, S. Brown-Leger, in preparation.
35. W. B. Curry, T. M. Marchitto, J. F. McManus, D. W. Oppo, K. L. Laarkamp, in *Mechanisms of Global Climate Change at Millennial Time Scales*, P. U. Clark, R. S. Webb, L. D. Keigwin, Eds. (American Geophysical Union, Washington, DC, 1999), vol. 112, p. 59.
36. T. F. Stocker, D. G. Wright, *Radiocarbon* **40**, 359 (1998).
37. M. Stuiver, H. A. Polach, *Radiocarbon* **19**, 355 (1977).
38. O. Marchal, T. F. Stocker, R. Muscheler, *Earth Planet. Sci. Lett.* **185**, 383 (2001).
39. A. Indermuhle, E. Monnin, B. Stauffer, T. F. Stocker, M. Wahlen, *Geophys. Res. Lett.* **27**, 735 (2000).
40. K. D. Alverson, R. S. Bradley, T. F. Pederson, Eds., *Paleoclimate, Global Change and the Future* (Springer Verlag, New York, 2003).
41. W. B. Curry, J.-C. Duplessy, L. D. Labeyrie, N. J. Shackleton, *Paleoceanography* **3**, 317 (1988).
42. W. S. Broecker, *Science* **300**, 1519 (2003).
43. This work was supported by NSF (OCE-0117356), Lawrence Livermore National Laboratory (LDRD-97-ERI-009), and the U.S. Department of Energy (W-7405-Eng-48). We thank the ODP Core Repository in Bremen for core sampling; B. Frantz and P. Zermeno for sample preparation assistance; C. Laj, M. Frank, J.-P. Valet, and J. Stoner for providing their data of past geomagentic field intensities; and S. Johnsen for making available the revised GRIPss09sea chronology. This is WHOI contribution no. 11061.

Supporting Online Material

www.sciencemag.org/cgi/content/full/303/5655/202/DC1
Materials and Methods
Figs. S1 to S4
Tables S1 and S2

11 August 2003; accepted 25 November 2003

REPORTS

Abiotic Forcing of Plankton Evolution in the Cenozoic

Daniela N. Schmidt,*† Hans R. Thierstein, Jörg Bollmann, Ralf Schiebel

We characterize the evolutionary radiation of planktic foraminifera by the test size distributions of entire assemblages in more than 500 Cenozoic marine sediment samples, including more than 1 million tests. Calibration of Holocene size patterns with environmental parameters and comparisons with Cenozoic paleoproxy data show a consistently positive correlation between test size and surface-water stratification intensity. We infer that the observed macroevolutionary increase in test size of planktic foraminifera through the Cenozoic was an adaptive response to intensifying surface-water stratification in low latitudes, which was driven by polar cooling.

A long-standing controversy surrounds the relative importance of biotic controls (such as competition, predation, grazing, and infection) versus abiotic forcing (such as climate, geography, bolide impacts, and volcanism) in shaping the evolution of life on Earth (*1*, *2*). A few exemplary morphometric studies of marine microfossils have focused on the ecological aspects of evolutionary change (*3*, *4*), although most have concentrated on the stratigraphic patterns of size and shape changes (*5*–*7*). Macroevolutionary processes—evolution above the species level—may be characterized by changes in diversity, longevity, speciation and extinction rates, and the size of fossil organisms (*8*). Body size, an easily measured indicator of macroevolution, is related to biological processes (*9*), notably metabolism, growth rate, and resistance to starvation and predation, and to environmental factors (*9*). However, little has been known about such relationships in the past. The dearth of data and consequently slow progress has mainly been due to the laboriousness of collecting morphometric measurements.

In order to avoid this difficulty, we have used automated microscopy (*10*) to measure the size distributions of entire planktic foraminiferal assemblages in 69 Holocene (*11*) and 454 Cenozoic (*12*) globally distributed deep-sea samples (for a total of 10^6 shells), from 18 high- and low-latitude Deep-Sea Drilling Program (DSDP) and Ocean Drilling Program (ODP) drill sites (table S1). All size spectra measured are from the >150-μm fractions and are strongly right-skewed. Means, maxima, and 95th percentiles are highly correlated with each other and generally increase with surface-water temperature (*11*). Following Chapelle and Peck (*13*), we used the 95th percentile, i.e., the size that separates the smaller 95% of individuals from the largest 5% (the $size_{95/5}$) (*11*, *14*). These size measurements allow us to address a very fundamental but still elusive question in paleobiology: Is the observed evolutionary size increase the result of a random increase in variance (*15*, *16*), or is it mainly due to biotic interactions (*1*) or to abiotic forcing (*2*)?

Since the early Cretaceous [~140 million years ago (Ma)], planktic foraminifera have undergone at least three episodes of major evolutionary radiation (*17*, *18*), each of which is thought to have involved increases in test size (*16*). These increases started at 132 Ma, 65 Ma, and 33 Ma (*16*). The main features of our data set on $size_{95/5}$ evolution of planktic foraminifera since the late Cretaceous are most apparent when grouped into low- and high-latitude averages for one-million-year (1-My) intervals (Fig. 1A). The major emerging characteristic is that $size_{95/5}$ development was coherent in both low- and high-latitude assemblages up to 42 Ma (mid-Eocene) and has diverged since. The sudden $size_{95/5}$ decrease at the Cretaceous/Paleogene boundary 65 Ma (*19*) was global and is linked to the impact-related mass extinction of most planktic foraminiferal species. In high-latitude records from the Kerguelen Plateau, Rockall Plateau, Walvis Ridge, and Rio Grande Rise, the $size_{95/5}$ of planktic foraminiferal assemblages remained dominantly small and never recovered to their late Cretaceous values (*12*). In low-latitude areas, the $size_{95/5}$ development can be divided into four time intervals based on the $size_{95/5}$ relationship to the Cenozoic mean ($size_{95/5}$ = 389 μm): an interval of dwarfed assemblages (65 to 59 Ma) until $size_{95/5}$ reached the Cenozoic average for the

Department of Earth Sciences, Eidgenössische Technische Hochschule (ETH) Zürich, and University of Zürich, ETH-Zentrum, CH-8092 Zürich, Switzerland.

*Present address: Department of Geology, Royal Holloway, University of London, Egham, Surrey TW20 OEX, UK.
†To whom correspondence should be addressed. E-mail: d.schmidt@gl.rhul.ac.uk